RSC Advances

PAPER

View Article Online
View Journal | View Issue

Check for updates

Cite this: *RSC Adv.*, 2026, **16**, 474

Biodegradable drug-eluting PLGA nanofiber scaffolds for long-term inhibition of colon cancer progression

Jiawei Xu,†[a] Chaohui Zhen,†[b] Muhammad Saif Ur Rahman,[a] Hao Chen,[ac] Ziwei Ren,[a] Xia Zebin,[a] Yuxin Jin,[a] Rui Liang[b] and ShanShan Xu *[a]

Localized and sustained drug delivery offers a promising approach to overcome systemic toxicity and short drug exposure associated with conventional colorectal cancer therapies. In this study, we developed electrospun poly(lactic-*co*-glycolic acid) (PLGA) fibrous scaffolds incorporating 5-fluorouracil (5-FU) for biodegradable, site-specific chemotherapy. Scaffolds containing 0%, 2.4%, 6%, and 10% (w/w) 5-FU were fabricated and characterized by scanning electron microscopy, showing uniform fibers with dose-dependent changes in diameter and surface texture. *In vitro* release studies revealed biphasic kinetics, characterized by an initial burst followed by sustained release over 35 days, thereby ensuring prolonged drug availability. Functional assays confirmed selective cytotoxicity against SW620 colorectal cancer cells. In an orthotopic tumor recurrence model, 5-FU-loaded scaffolds, particularly at higher doses, markedly suppressed tumor growth and reduced recurrence. Histological analysis showed disrupted tumor structure, decreased proliferation (Ki-67), reduced angiogenesis (CD31), and diminished extracellular matrix remodeling (fibronectin). Body weight remained stable, indicating minimal systemic toxicity. Together, these findings demonstrate that 5-FU-loaded PLGA scaffolds provide localized, long-term tumor suppression with high spatial precision and low systemic burden, highlighting their potential for post-surgical colorectal cancer therapy.

Received 25th September 2025
Accepted 1st December 2025

DOI: 10.1039/d5ra07276j

rsc.li/rsc-advances

Open Access Article. Published on 02 January 2026. Downloaded on 4/7/2026 1:57:52 AM.
This article is licensed under a Creative Commons Attribution-NonCommercial 3.0 Unported Licence.

1 Introduction

The global burden of colon cancer has continued to escalate, with 1.93 million new cases reported in 2020, representing 9.6% of all cancer diagnoses.[1] Although the adoption of colonoscopy screening has improved early detection, late-stage colon cancer remains challenging to treat due to deep tumor infiltration and involvement of critical vascular and neural structures.[2,3]

Historically, systemic chemotherapy formed the cornerstone of treatment, employing agents such as oxaliplatin, capecitabine, 5-fluorouracil (5-FU), irinotecan, and bevacizumab,[4] The widely implemented FOLFOX regimen, comprising oxaliplatin 85 mg m^{-2}, folic acid calcium 400 mg m^{-2}, and 5-FU in both bolus and continuous infusion forms, has provided measurable clinical benefit.[5]

However, as clinical experience accumulated, the limitations of systemic drug delivery became increasingly apparent. Non-specific biodistribution, rapid blood clearance, cumulative toxicity, and the emergence of chemoresistance severely restricted the long-term efficacy of these therapies.[6] In response, research from the late 20th century onward shifted toward localized treatment strategies such as hyperthermic perfusion,[7] implantable infusion pumps,[8] and microsphere-based carriers.[9] Yet concerns regarding the biocompatibility and clinical safety of several carrier systems[10,11] motivated the search for more advanced biomaterials.

This search led to the development of modern drug-delivery systems (DDSs), including liposomes, hydrogels, and fibrous meshes, each designed to enhance therapeutic precision and reduce systemic toxicity.[12] With increasing material sophistication, poly(lactic-*co*-glycolic acid) (PLGA) emerged as a leading candidate due to its FDA approval, biocompatibility, and tunable degradation.[13,14] Electrospinning technologies further enhanced the capabilities of PLGA films for controlled drug release.[15,16] However, early PLA-based systems still faced challenges such as burst release and limited drug-release duration[17,18].

More recently, electrospun nanofibers have become central to the development of localized postoperative therapies, offering large surface areas, enhanced loading capacity, structural tunability, and ECM-like architecture.[19–24]

[a]*Institute for Advanced Study, Shenzhen University, Shenzhen 518060, China. E-mail: xuss@szu.edu.cn*

[b]*Department of Gastrointestinal Surgery, The First Dongguan Affiliated Hospital, Guangdong Medical University, Dongguan, Guangdong 523710, China*

[c]*Department of Mechanical and Aerospace Engineering, The George Washington University, D.C. 20052, Washington, USA*

† Jia Wei, Chaohui Zhen contributed equally.

© 2026 The Author(s). Published by the Royal Society of Chemistry

Open Access Article. Published on 02 January 2026. Downloaded on 4/7/2026 1:57:52 AM. This article is licensed under a Creative Commons Attribution-NonCommercial 3.0 Unported Licence.

Given these unmet challenges, there is a clear need for a biodegradable, biocompatible, and precisely controlled local drug-delivery platform capable of sustaining adequate chemotherapeutic exposure at the tumor resection site while minimizing systemic toxicity. Therefore, this project aimed to develop an electrospun 5-FU-loaded PLGA nanofiber scaffold designed to regulate the local microenvironment and achieve controlled, long-term drug release. We fabricated drug-loaded membranes with varying drug concentrations, evaluated their loading capacity, release kinetics, and biocompatibility, and assessed their ability to suppress colon cancer cell proliferation and tumor progression both *in vitro* and *in vivo*. Through this work, we aim to establish a robust and clinically relevant foundation for precision, localized therapy in the management of colon cancer.

2 Materials and methods

2.1 Materials and reagents

PLGA (MW = 60 000 Da, LA/GA = 75/25) was purchased from Evonik Industries AG. 5-Fu was purchased from Zhuoke (Hainan). *N*, *N*-Dimethylformamide (DMF) and acetone were obtained from Sinopharm Chemical Reagent Co., Ltd Phosphate-buffered saline (PBS, pH = 7.4) was purchased from Huankai Microbiology Technology Co., Ltd (Guangdong, China). All other chemicals were obtained from commercial sources in reagent grade and used without further purification.

2.2 Composition of drug-loaded electrospun fibrous membranes

5-Fu drug-loaded fibrous membranes were created using an electrospinning technique and solvent evaporation. Table 1 presents the chemical composition of the electrospun membrane. 0% 5-FU, 2.4% 5-FU, 6% 5-FU, and 10% 5-FU were loaded into PLGA electrospun fibrous membrane.

2.2.1 Solution preparation. The drugs were initially dissolved in acetone and DMF. The drug-dissolved solution received the addition of the PLGA powder. Magnetic stirring completely dissolved the combined polymer solution. The concentration in both polymer solutions was 45–50% (mPolymer [g] per Vsolution [mL]). The mixed drug-dissolved polymer solution was magnetically stirred at 25 °C (room temperature) for 6 h to create a homogeneous drug-polymer solution.

2.2.2 Electrospinning of drug-loaded fibrous membrane. The electrospinning device used in this experiment primarily consists of a feeding device, a propeller, a high-voltage power supply, and a collector. Take the PLGA powder and dissolve it in a mixed solvent of DMF and ACE (DMF: ACE = 6:4). After 6 hours of magnetic stirring, a transparent homogeneous solution was formed. Then, different masses of 5-FU drug powder were added and stirred for 2 hours to ensure the drug was completely dissolved in the solution. Transfer the polymer solution to an injection syringe to prepare for electrospinning. The electrospinning environment remains unchanged. The temperature is 25 ± 2 °C, and the humidity is 50 ± 5%. The electrospinning voltage range was 24–40 kV, the propelling rate range was between 10–40 μL min^{-1}, and the receiving distance ranged from 18–28 cm. The thickness of all fiber membranes is controlled within 100 ± 15 μm. After electrospinning, the collected electrospun fiber membranes were vacuum-dried for 72 hours, allowing the residual solvents to evaporate completely.[25]

Table 1 Four groups of drug-loaded fibrous membranes[a]

Group	Solvent	Polymer	Drug	Concentration
1	DMF : ACE = 6 : 4	PLGA7525	5-FU	0%
2	DMF : ACE = 6 : 4	PLGA7525	5-FU	2.4%
3	DMF : ACE = 6 : 4	PLGA7525	5-FU	6%
4	DMF : ACE = 6 : 4	PLGA7525	5-FU	10%

[a] DMA: dimethylformamide, ACE: acetone.

2.3 Characterization of the drug-loaded electrospun membranes

2.3.1 Scanning electron microscopy. Drug-loaded membranes were observed under scanning electron microscopy SEM (Phenom Pro, Japan) with and without PBS incubation. Membranes were sputtered with gold to observe the surface and cross-sectional morphologies of the scaffold.

2.3.2 Differential scanning calorimetry (DSC) analysis. The test samples were prepared by dissolving the substance in an appropriate solvent and sealing them in aluminum pans for DSC analysis. Approximately 10–15 mg of each sample was used to ensure consistency across all measurements. DSC measurements were performed using a calibrated instrument (PerkinElmer, DSC 8500) with a heating rate of 10 °C min^{-1} from 0 °C to 100 °C under a nitrogen atmosphere at a flow rate of 50 mL min^{-1}. The heat flow (mW) *versus* temperature (°C) data were recorded for each sample.

2.3.3 Fourier transform infrared (FTIR) spectroscopy. FTIR spectroscopy was employed to investigate potential molecular interactions between PLGA and 5-FU and to confirm the presence of the drug within the polymer matrix. Samples analyzed included pPLGA, 5-FU, and PLGA-5-FU of 2.4%, 6%, and 10% (w/w) relative to polymer. Electrospun mats or cast films were cut into small pieces to obtain representative regions and then gently dried under ambient conditions to minimize residual moisture before analysis.

Spectra were recorded using an FTIR spectrometer. The spectra were acquired over the mid-infrared range that encompasses the principal vibrational modes of PLGA and 5-FU. For each specimen, multiple scans were averaged to improve the signal-to-noise ratio, and a background spectrum was collected under the same conditions and automatically subtracted. All spectra were processed using the instrument software, which included baseline correction and normalization, allowing for direct comparison of band positions and relative intensities among formulations.

2.3.4 Mechanical testing of PLGA/5-FU composite films. The mechanical properties of blank and PLGA incorporated with varying concentrations of 5-FU, 2.4%, 6%, and 10%, were evaluated using tensile testing. The tensile tests were performed

Open Access Article. Published on 02 January 2026. Downloaded on 4/7/2026 1:57:52 AM. This article is licensed under a Creative Commons Attribution-NonCommercial 3.0 Unported Licence.

on Discovery DMA850 (TA Instruments) at a crosshead speed of 5 mm min^{-1}. The stress–strain behavior was recorded by stretching each sample until failure, and the maximum stress (tensile strength) and elongation at break (strain) were determined. Each group was tested in triplicate to ensure statistical validity. The tensile strength (MPa) and strain (%) data were analyzed to assess the effects of 5-FU concentration on the mechanical properties of PLGA films.

2.3.5 Contact angle measurement of PLGA films. Static water contact angle measurements were performed by Attension Theta Flex (Biolin, Theta) to evaluate the surface wettability of PLGA films containing different concentrations of incorporated additive (Blank, 2.4%, 6%, and 10%). Uniform PLGA films were prepared and allowed to equilibrate under ambient laboratory conditions before analysis to ensure stable surface properties. A droplet of deionized water was gently dispensed onto the surface of each film, and high-resolution side-view images were captured immediately following droplet placement. The contact angle was determined by fitting the recorded droplet profile with a standard ellipsoidal or circular-arc model using the instrument's software. Contact angle values were expressed as the mean of replicate measurements for each concentration group.

2.3.6 Polymer degradation study. A degradation study was conducted to assess the morphological changes of polymer scaffolds over time in an aqueous environment designed to simulate physiological conditions. Pre-fabricated scaffolds were cut into uniform sections to ensure comparable surface area and thickness across all samples. Each scaffold sample was immersed in PBS to maintain a stable pH and temperature throughout the experiment. The medium was refreshed periodically to prevent the accumulation of degradation by-products that could influence surface morphology. At predetermined intervals, samples were gently removed from the medium, briefly rinsed to eliminate loosely bound residues, and allowed to dry under controlled conditions to avoid deformation or collapse of the polymer network. After drying, the samples were analysed by SEM. Micrographs were analyzed qualitatively to observe changes in fiber thickness, network integrity or fragmentation.

2.3.7 *In vitro* drug release experiment. We weighed 0.01 g of 5-FU, dissolved it with PBS solution first, and then prepared the drug stock solution in a 100 mL volumetric flask. The stock solution was diluted to different concentrations, and the absorbance was measured at 266 nm (for 5-FU) using UV-Vis spectroscopy to obtain the 5-FU drug standard curve.

The drug-loaded fiber membrane was cut to a 1.5 × 1.5 cm^2 area, fixed with a special clip, and immersed in 5 mL of PBS solution. The sample was placed in a 37 °C constant temperature shaker at 100 rpm. At fixed time points, the drug release solution was removed, and the concentration of 5-FU in the solution was measured using UV-Vis spectroscopy. By measuring the drug concentration at different time points, the drug release curve was plotted to analyze the release rate and mechanism of the drug.[25,26]

2.4 *In vitro* inhibition of tumor cells

2.4.1 Cell cultures. Colon cancer cells (SW620) and colonic epithelial cells (NCM460) were purchased from Procell. The SW620 cells were cultured in Dulbecco's modified Eagle's medium supplemented with 10% (v/v) fetal bovine serum and 1% (v/v) penicillin-streptomycin at 37 °C in humidified culture conditions (95% humidity) with 5% CO_2. The NCM460 cells were cultured in RPMI 1640 medium supplemented with 10% (v/v) fetal bovine serum and 1% (v/v) penicillin-streptomycin at 37 °C in humidified culture conditions (95% humidity) with 5% CO_2. When cells reached about 90% confluency, they were passaged.[27]

2.4.2 *In vitro* cytotoxicity test. Fig. 3A illustrates that the collar consists of two rings: an upper and a lower ring. The fiber membranes were prepared for 24 h, 72 h, and 168 h according to the ISO10993-5 standard for biological evaluation of medical devices, with the material extract solution having a surface area to culture medium volume ratio of 3 cm mL^{-1}. In a 96-well plate, NCM460 and SW620 cells were inoculated at densities of 1×10^4 and 5×10^4 cells per well, respectively. After 24 hours of cultivation, 24 h, 72 h, and 168 h, cell viability was detected using the CCK-8 method, and the CCK-8 reagent was prepared at a 1:10 dilution with either DMEM or RPMI culture medium, depending on the cell type. 100L of the mixed solution was added to each well, and the plate was incubated at 37 °C in the dark for 60 minutes. The absorbance at 450 nm was measured using an enzyme-linked immunosorbent assay (ELISA) reader. The cell survival rate was calculated as (experimental group OD value/negative control group OD value) × 100%, and three independent experiments were conducted.[28]

2.4.3 Live/dead staining. The fiber membranes were cut to 1.5 × 1.5 cm^2 and fixed using the collar before being placed in a 24-well plate. NCM460 and SW620 cells were inoculated onto the fiber membranes for cultivation. The plate was removed at 24 hours, 72 hours, and 168 hours of cultivation. The live/dead staining mixture solution was prepared at a ratio of PBS:AM: PI = 1000:3:2. 200 mL of the staining solution was added to each well, and the plate was incubated in the dark for 15 minutes. The plate was washed three times with PBS to remove free dyes. The cells were observed using a laser confocal microscope to observe the survival status of the cells on the fiber membranes. The AM reagent labels living cells, which appear green at a wavelength of 488 nm. PI labels dead cells, which appear red at a wavelength of 561 nm.

2.5 Establishment of the tumor xenograft

All animal procedures were performed in accordance with the Guidelines for Care and Use of Laboratory Animals of Shenzhen University and approved by the Animal Ethics Committee of the IACUC.

The 6-week-old BALB/c female mice were purchased from the Guangdong Medical Laboratory Animal Center. All mice were maintained in a specific pathogen-free (SPF) barrier facility at the Shenzhen University Laboratory Animal Center. The mice were maintained on a 12-hour light/12-hour dark cycle at 22–26 °C, with sterile pellet food and water available ad libitum. All animal protocols used in this study were approved by the Institutional Animal Care and Use Committee (IACUC) of Shenzhen University.

© 2026 The Author(s). Published by the Royal Society of Chemistry

Open Access Article. Published on 02 January 2026. Downloaded on 4/7/2026 1:57:52 AM. This article is licensed under a Creative Commons Attribution-NonCommercial 3.0 Unported Licence.

SW620 cells were collected and washed twice with cold PBS. 3×10^6 SW620 cells suspensions in cold PBS were injected into the rear flank of the mice. A vernier caliper was used to measure the length and width every two days, and tumor size was calculated using the following formula. Tumor volume (mm^3) = 1/2 × length (L) × width (W).[2] The animal's body weight was measured by an electronic balance every two days. Mice with 180–200 mm^3 tumor sizes were selected for the formal animal experiment.

2.5.1 Tumor model grouping and treatments. Fig. 4A shows the schematic diagram of tumor excision and scaffold implantation in the mouse subcutaneous tumor model. After injecting the cells and waiting for the mice to form tumors, when the tumor volume reaches the volume criteria for inclusion in the study, the basement membrane excision surgery is performed, and different materials are implanted according to the corresponding groups. The specific experimental groups and surgical requirements are as follows: the wild-type group was not inoculated with tumor cells. The control group was inoculated with SW620 colon cancer cells without any treatment. The Basement membrane resection (BMR) group: inoculated with SW620 colon cancer cells, and when the tumor grew to approximately 200 mm^3, the tumor was surgically removed to the remaining layer of the basement membrane, resulting in a remaining tumor tissue volume of roughly 4 mm^3 (the remaining tumor tissue volume was 1–2% of the original tumor volume, which could simulate the scenario where clinical surgery could not completely remove the tumor). The tail vein injection group (IV): inoculated with SW620 colon cancer cells, when the tumor grew to approximately 200 mm^3, a BMR resection surgery was performed. On the first day after surgery, a tail vein injection of 5-FU drug treatment was administered, with a drug concentration of 2.5 mg kg^{-1}, repeated every three days.[29] The other groups were inoculated with SW620 colon cancer cells, and when the tumor grew to approximately 200 mm^3, different concentrations of PLGA-5-FU fiber membranes were implanted after basal membrane resection as shown in Table 2.

2.5.2 Hematoxylin and eosin (H&E) staining. H&E staining was performed according to the standard protocol for pathological examination of the tissues. After the mice were sacrificed, the heart, liver, spleen, lung, kidney, and tumor were fixed in 4% paraformaldehyde. Tissues were dehydrated in gradient ethanols, cleared in xylene, and embedded in paraffin. The tissue blocks were sectioned at a thickness of 4–5 μm and used for histological analysis. H&E staining of tissue paraffin sections is performed by dewaxing in xylene, hydrating through gradient ethanol, H&E staining, and dehydration in gradient alcohol and xylene. A pathologist used light microscopy to examine the H&E-stained slides (Nikon U-III multipoint sensor system).

2.5.3 Immunohistochemistry. The paraffin sections were successively immersed in xylene I, II, and III for 5 minutes each for dewaxing. Then, they were hydrated in a gradient of ethanol (100%, 95%, 90%, 75%) for 5 minutes each, followed by rinsing with running water for 5 minutes to remove residual organic solvents. Next, the sections were treated with 3% H_2O_2 at room temperature for 10 minutes to block endogenous peroxidase activity, washed three times with PBS, and then subjected to high-temperature and high-pressure antigen retrieval using a sodium citrate buffer (pH 6.0). After natural cooling to room temperature, they were washed three times with PBS. A 5% BSA blocking solution was added at room temperature for 20–30 minutes to block non-specific binding sites. After removing the blocking solution, one-antibody dilutions (Ki-67, CD31, Fibronectin) were added at 4 °C for overnight incubation. After PBS washing three times, an HRP-labeled secondary antibody was added at room temperature for 30 minutes. The reaction was terminated when the positive signal appeared brown under the microscope using DAB staining solution. The cells were stained with hematoxylin for 5 minutes, then differentiated with a differentiation solution, rinsed with running water, and counterstained with blue. Finally, the sections were dehydrated in a gradient of ethanol (75%, 95%, 95%, 100%, 100%) for 5 minutes each, then transparentized with xylene three times and cover slip was mounted.

2.6 Statistical analysis

All experiments were performed at least three times to satisfy minimal statistical significance. The results are shown as the mean ± SD. Student's t-test produced significant differences between groups; $p < 0.05$ was considered statistically significant, and $p < 0.01$ was considered highly significant.

3 Results and discussion

3.1 Successful fabrication of uniform PLGA and drug-loaded fibrous scaffolds

Electrospinning enabled the successful fabrication of blank and 5-fluorouracil (5-FU)-loaded PLGA fibrous membranes, schematically depicted in Fig. 1A. The fibers were generated using a controlled electrospinning process from a PLGA solution in a DMF: acetone (6 : 4) solvent system with varying drug concentrations (0%, 2.4%, 6%, and 10% w/w).

Table 2 Animal experiment grouping

No.	Group	Operation	Duration
1	Wild type	No treatment, no tumor	—
2	Control	Tumor-bearing, untreated	—
3	BMR	Resection	—
4	IV	Resection, tail vein 5-FU, 2.5 mg kg^{-1}	Every 3 days, once
5	PLGA Blank	Resection, 0% 5-FU	Implanted once
6	PLGA low 5-FU	Resection, 2.4% 5-FU	Implanted once
7	PLGA high 5-FU	Resection,10% 5-FU	Implanted once

Open Access Article. Published on 02 January 2026. Downloaded on 4/7/2026 1:57:52 AM.
This article is licensed under a Creative Commons Attribution-NonCommercial 3.0 Unported Licence.

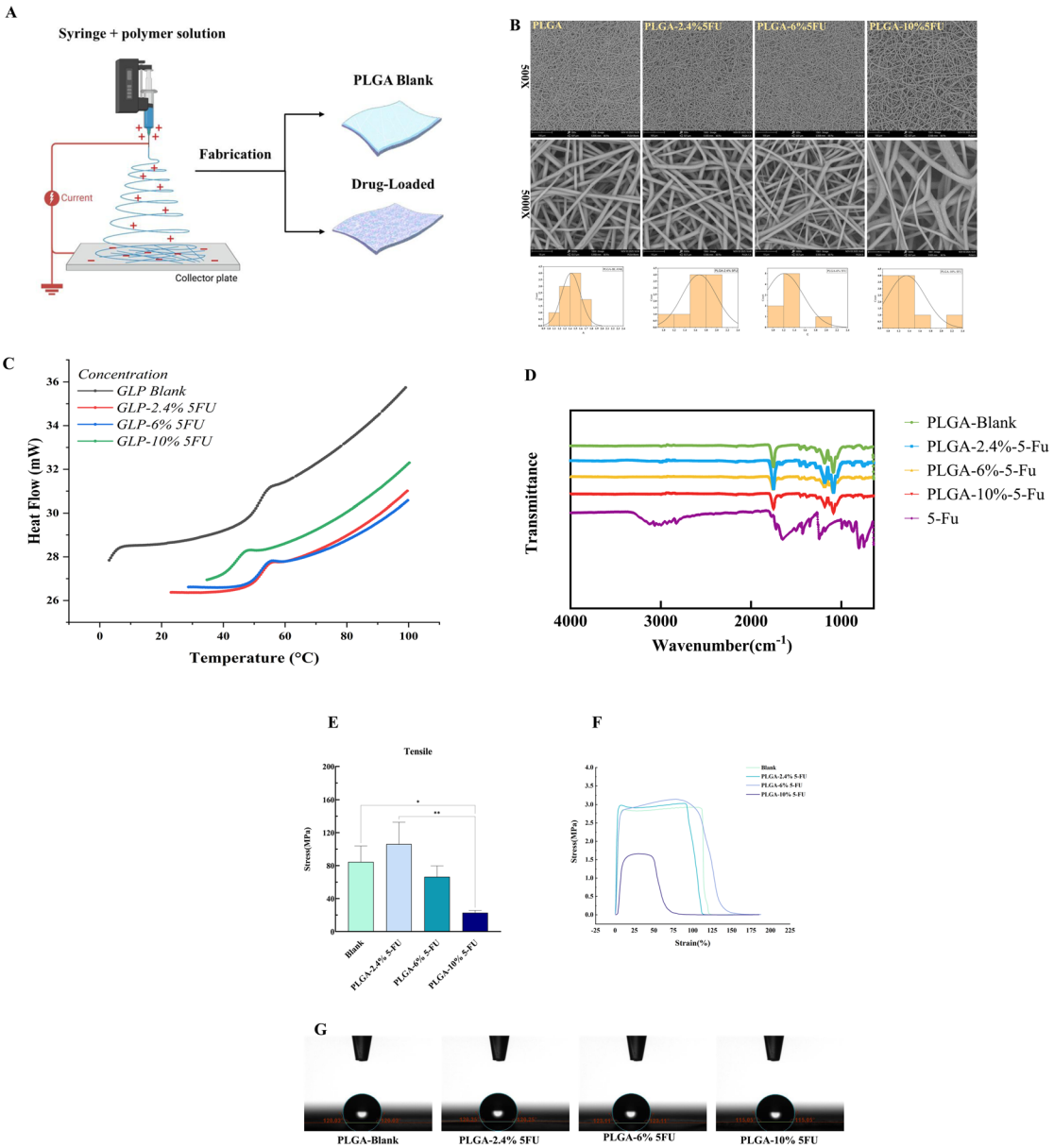

Fig. 1 Fabrication, morphological characterization, and drug release profile of 5-Fu-loaded PLGA electrospun scaffolds. (A) Schematic representation of the electrospinning process used to fabricate blank and 5-Fu-loaded PLGA fibrous scaffolds. (B) SEM analysis showing the morphology of blank PLGA fibers and scaffolds loaded with different concentrations of 5-Fu (2.4%, 6%, and 10%), with corresponding fiber diameter distribution histograms. (C) DSC Thermal Transition Heat flow (mW) was measured as a function of temperature (°C) for four sample conditions: PLGA-Blank, PLGA-2.4% 5-FU, PLGA-6% 5-FU, and PLGA-10%. All samples display an increase in heat flow with rising temperature, with higher concentrations generally exhibiting elevated heat-flow values compared to lower concentrations. The blank shows the highest overall heat flow across the temperature range, while the 2.4% and 6% curves follow similar trends with slight divergence at higher temperatures. The 10% sample demonstrates intermediate heat-flow behavior, increasing steadily from ~35 °C onward. (D) FTIR spectra are shown for PLGA-Blank (green), PLGA-2.4%-5-Fu (blue), PLGA-6%-5-Fu (orange), PLGA-10%-5-Fu (red), and pure 5-Fu (purple). All spectra were collected in the mid-infrared region and plotted as transmittance *versus* wavenumber (cm^{-1}). The PLGA-Blank spectrum exhibits the characteristic ester carbonyl band and C–O–C stretching vibrations of the polyester backbone. The 5-Fu spectrum displays distinct carbonyl and ring-stretching bands typical of the fluoropyrimidine structure. In the drug-loaded PLGA samples, polymer bands dominate while additional 5-Fu-related peaks become progressively more pronounced as the nominal drug content increases from 2.4% to 10%, confirming successful incorporation of 5-Fu into the matrix. The absence of new bands suggests that no major chemical reaction occurs between PLGA and 5-Fu and that the drug is physically dispersed within the polymer. (E and F) Dynamic Mechanical Analysis (DMA) stress–strain curves of PLGA films containing different concentrations of 5-FU (0%, 2.4%, 6%, and 10%). Increasing 5-FU content reduced the tensile strength and elongation of the films. Comparison of tensile stress of PLGA films with varying 5-FU concentrations. * and ** indicate statistically significant differences compared to the Blank group (*$p < 0.05$, **$p < 0.01$). (G) Contact angle measurements. Representative static water droplet images for PLGA-Blank, PLGA-2.4% 5-FU, PLGA-6% 5-FU, and PLGA-10% 5-FU films are shown. Contact angles derived from droplet profile fitting are indicated at the base of each image. The PLGA-Blank and PLGA-2.4% samples display similar contact angles (~120°), consistent with hydrophobic surfaces. The PLGA-6% film shows a slight increase in hydrophobicity (~123°), whereas the PLGA-10% film demonstrates a notable decrease (~115°), indicating enhanced wettability at higher additive content.

© 2026 The Author(s). Published by the Royal Society of Chemistry

Open Access Article. Published on 02 January 2026. Downloaded on 4/7/2026 1:57:52 AM.
This article is licensed under a Creative Commons Attribution-NonCommercial 3.0 Unported Licence.

The 5-FU concentrations used in this study were chosen to align the scaffold's drug content with clinically and preclinically relevant exposure ranges while enabling a controlled assessment of dose–response effects. In clinical practice, 5-FU is administered according to body surface area to approximate mg kg^{-1} equivalents. When translated to murine models using standard allometric considerations, published studies commonly employ doses ranging from ~20–100 mg kg^{-1}, indicating that therapeutically meaningful exposures in mice also lie within this range.[30–32]

Based on these clinical-to-preclinical reference values, the scaffold loadings of 2.4%, 6%, and 10% (w/w) were selected to represent low, intermediate, and high drug-dose conditions. These loading levels are designed so that, for a typical scaffold mass and release profile, the total amount of released 5-FU falls within or near the therapeutic window when normalized to body weight. The lowest loading (2.4%) approximates a conservative, clinically relevant exposure; the intermediate loading (6%) explores potential dose-dependent improvements in efficacy; and the highest loading (10%) evaluates the upper practical limit of drug incorporation without compromising fiber morphology or mechanical integrity. The unloaded scaffold (0%) provides an essential control and its role without any drugs.

Together, this graded loading scheme allows systematic investigation of the influence of 5-FU dose on release kinetics, tissue response, and functional outcomes, while maintaining translational relevance to established human and murine dosing paradigms. The resulting scaffolds maintained uniform thickness (~100 ± 15 μm) and integrity post-drying, illustrating the feasibility of incorporating chemotherapeutic agents into polymeric carriers without compromising structural formation.

The rationale for developing a localized intraoperative single drug delivery system extends beyond maintaining therapeutic drug levels at the tumor bed. Systemic administration of 5-FU, although clinically effective, is limited by rapid systemic clearance, short plasma half-life, and dose-limiting toxicities that restrict the achievable therapeutic window. As a consequence, only a small fraction of the administered dose reaches the surgical resection site, where microscopic residual tumor cells are most likely to persist. In the context of this work, the purpose of incorporating 5-FU into an electrospun PLGA scaffold is not solely to sustain local drug concentrations but to exploit the intrinsic physicochemical properties of the scaffold to potentiate the antitumor activity of 5-FU. Electrospun fibers provide high surface area, tunable degradation kinetics, and a microstructured architecture that can modulate local pH, diffusion behavior, and cellular interactions. These features have been demonstrated to impact tumor cell proliferation, invasion, and apoptosis pathways. They can act synergistically with chemotherapeutic agents by enhancing local uptake, prolonging exposure, or sensitizing tumor cells to drug-induced cytotoxicity. Thus, the scaffold functions as an active therapeutic component, not merely a passive carrier. By combining these scaffold-driven biophysical effects with controlled 5-FU release, our system aims to achieve enhanced antitumor efficacy at lower drug doses, thereby reducing the systemic toxicity commonly associated with conventional chemotherapy. This strategy aligns with emerging approaches in local oncology therapeutics, where rationally engineered biomaterials are designed to amplify drug potency while limiting adverse effects.

3.1.1 Drug loading alters fiber diameter and surface morphology. SEM analysis revealed that all fibrous membranes exhibited smooth, bead-free, and randomly oriented fibers (Fig. 1B). Blank PLGA fibers showed narrow diameter distributions and soft surfaces. With increasing drug content, particularly at 6% and 10% 5-Fu (Fig. 1B, lower panel), the fiber morphology shifted to display larger, more heterogeneous diameters and increased surface roughness. The highest drug-loaded group (10% 5-Fu) showed occasional fiber fusion and a broader distribution, suggesting that elevated drug concentration influences fiber solidification dynamics and surface characteristics. These observations confirm a dose-dependent effect of drug incorporation on fiber morphology and architecture. The porous, non-woven architecture of the scaffolds was preserved irrespective of drug loading, suggesting their suitability for biomedical applications requiring high surface-area-to-volume ratios.

3.1.2 Effect of sample concentration on heat flow across increasing temperature. DSC analysis revealed distinct, concentration-dependent modifications in thermal behavior across the GLP formulations (Fig. 1C). The GLP blank displayed a comparatively linear heat-flow profile, with only a gradual increase in endothermic signal across the examined temperature range, consistent with baseline polymer relaxation processes.

In contrast, incorporation of 5-FU induced measurable thermal perturbations. The 2.4% 5-FU formulation exhibited a modest elevation in heat flow relative to the blank, indicating the onset of weak thermal transitions, potentially associated with localized molecular rearrangements or low-level polymer–drug interactions. Increasing the drug loading to 6% produced a more pronounced deviation, characterized by a steeper rise in heat flow and a clearer inflection in the 50–70 °C region. This behavior suggests more substantial thermotropic changes, such as partial phase reorganization or increased disruption of the polymeric network as drug–polymer interactions intensify.

The 10% 5-FU formulation demonstrated the most significant enhancement in endothermic response, with a well-defined thermal event evident over the same temperature interval. The magnitude of this shift indicates substantial modification of the polymer matrix, consistent with higher degrees of molecular interaction and potential formation of new microstructural arrangements at elevated drug loadings. Collectively, the progressive increase in heat-flow intensity with concentration supports the hypothesis that drug incorporation alters the thermal stability and transition behavior of GLP in a dose-dependent manner.

3.1.3 FTIR characterization of PLGA/5-Fu systems. FTIR spectroscopy was employed to evaluate the chemical stability of the PLGA matrix and to verify the successful incorporation of 5-FU within the scaffolds. The spectral data are presented in Fig. 1D. The FTIR spectrum of the blank PLGA exhibited characteristic absorption bands corresponding to the ester carbonyl

Open Access Article. Published on 02 January 2026. Downloaded on 4/7/2026 1:57:52 AM.
This article is licensed under a Creative Commons Attribution-NonCommercial 3.0 Unported Licence.

(C═O) stretching vibration at ~1755 cm^{-1}, C–O–C stretching vibrations in the 1180–1085 cm^{-1} range, and aliphatic C–H stretching between 2950–2850 cm^{-1}. The absence of extraneous peaks confirmed that no chemical degradation of the polymer occurred during the fabrication process.

In contrast, the spectrum of pure 5-FU was distinct, featuring two sharp carbonyl stretching bands at 1685–1660 cm^{-1}, attributable to the C═O and C–F groups, alongside a series of vibrations between 1250–1000 cm^{-1} associated with the heterocyclic ring structure. Analysis of the PLGA-5-FU composite scaffolds revealed a combination of these spectral features. The dominant ester carbonyl peak of PLGA remained consistently present at approximately 1755 cm^{-1} across all drug-loaded formulations. However, with increasing 5-FU loading, the characteristic drug carbonyl band at ~1680 cm^{-1} emerged and intensified. Quantitatively, at a 2.4% (w/w) drug loading, this band appeared as a low-intensity shoulder, representing a 5–8% increase in absorption relative to the PLGA-Blank baseline. A 6% loading resulted in a further 15–20% intensification of this band. At the maximum loading of 10%, the ~1680 cm^{-1} peak became a prominent feature, showing a greater than 35% increase in intensity compared to the 6% formulation.

Critically, the PLGA carbonyl peak exhibited only negligible shifts (1–3 cm^{-1}), and no new functional group absorptions or peak splitting were observed. This spectral evidence indicates the absence of covalent bonding between the polymer and the drug. The minimal wavenumber shifts in hydrogen-bond-sensitive regions suggest that any polymer–drug interactions are weak and non-covalent in nature. This is consistent with a mechanism of physical encapsulation, wherein 5-FU is molecularly dispersed within the polymer matrix without chemical modification.

In conclusion, the FTIR results quantitatively demonstrate that 5-FU is incorporated into the PLGA scaffold in its intact molecular form, with a direct correlation between its spectral signature and the nominal drug loading. The preservation of the PLGA backbone structure confirms the chemical stability of the polymer, thereby supporting the potential of these composite formulations for controlled drug-release applications. Together, DSC and FTIR findings underscore the strong coupling between drug loading and matrix thermodynamics.

3.1.4 Effect of 5-FU loading on the tensile properties of PLGA films. The tensile stress–strain curves (Fig. 1D) display the deformation characteristics of the blank and PLGA-5-FU composite films. The blank sample exhibited a higher tensile strength compared to the PLGA films with increasing concentrations of 5-FU. The stress at failure for the blank was around 3 MPa, while the PLGA films with 2.4% and 6% 5-FU showed comparable tensile strengths of approximately 1.5 MPa and 1.3 MPa, respectively. However, the PLGA film with 10% 5-FU exhibited the lowest tensile strength, reaching only about 0.6 MPa. The corresponding strain values indicated a noticeable increase in elasticity (strain at failure) for the PLGA-2.4% and PLGA-6% 5-FU films, with the PLGA-10% 5-FU film showing a dramatic reduction in strain (decreased flexibility), which correlates with the decrease in tensile strength.

Fig. 1E illustrates the tensile strength for each group. Statistical analysis revealed significant differences between the groups, with the blank showing significantly higher tensile strength compared to the PLGA-6% 5-FU films ($p < 0.05$*). Furthermore, the tensile strength of PLGA-2.4% 5-FU and PLGA-6% 5-FU films was significantly higher than that of the PLGA-6% 5-FU, as denoted by the double asterisk ($p < 0.01$**). The reduced mechanical properties of the PLGA-10% 5-FU film can be attributed to the plasticizing effect of higher 5-FU concentrations, which likely disrupted the polymeric structure, reducing the overall strength and elongation capacity. These results highlight the concentration-dependent influence of 5-FU on the mechanical properties of PLGA films.

3.1.5 Effect of additive concentration on the surface wettability of PLGA films. The contact angle images revealed apparent differences in the wettability of PLGA films as the drug concentration increased. The PLGA-Blank sample displayed a relatively high contact angle of approximately 120°, indicating a hydrophobic surface typical of unmodified PLGA. The introduction of a 1.2% additive concentration resulted in a contact angle nearly identical to that of the blank (~120.25°), demonstrating that minor incorporation did not substantially influence surface hydrophobicity.

A more noticeable change occurred at the 6% concentration, where the contact angle increased slightly to ≈123°. This modest rise suggests that the additive at this level may enhance surface hydrophobicity, potentially through changes in surface energy or the distribution of hydrophobic domains within the polymer matrix. Interestingly, the highest concentration, 10%, produced a lower contact angle (≈115°) compared to all other samples. This reduction implies that beyond a certain threshold, higher additive content may alter the film's microstructure in a manner that increases surface wettability. Possible explanations include migration of hydrophilic moieties to the surface, changes in polymer chain mobility, or alterations in surface roughness.

Overall, these results suggest a non-linear relationship between additive concentration and PLGA surface wettability, where moderate incorporation slightly increases hydrophobicity, but higher loading reverses this trend. Such findings provide insight into how formulation changes may influence interfacial behavior, which is critical for applications such as controlled drug release, cell–material interactions, and coating technologies.

3.2 Drug release and degradation

3.2.1 Morphological evolution of polymer scaffolds during degradation. The series of SEM micrographs revealed distinct degradation behaviors among the polymer scaffolds, each displaying progressive structural changes characteristic of hydrolytic or bulk erosion mechanisms. Initially, all scaffolds exhibited well-defined architectures, including interconnected fibrous networks or porous matrices, depending on the formulation. These initial morphologies served as the reference for evaluating subsequent degradation-induced transformations.

© 2026 The Author(s). Published by the Royal Society of Chemistry

Open Access Article. Published on 02 January 2026. Downloaded on 4/7/2026 1:57:52 AM.
This article is licensed under a Creative Commons Attribution-NonCommercial 3.0 Unported Licence.

Over the course of the degradation period, 3, 35, and 90 days, samples with highly fibrous structures demonstrated gradual thinning of fibers, nodular surface textures, and localized breakage. The interconnected fiber mats began to lose tension, forming loose or collapsed networks as polymer chains cleaved and mass loss progressed. In contrast, scaffolds with larger pores exhibited widening cavities, smoothed surfaces, and partial merging of pore walls, indicating the softening and relaxation of the matrix prior to fragmentation.

Some formulations displayed signs of accelerated degradation, where the originally continuous surfaces disintegrated into fragmented or plate-like debris. This behavior indicates material-dependent sensitivity to water penetration and chain scission, leading to faster structural collapse. The extent of change varied across samples, implying that polymer composition, additive concentration, or fabrication method strongly influence degradation stability.

Overall, the SEM observations confirm that the degradation pathway involves a shift from ordered microstructures to increasingly disorganized morphologies. Such transitions have significant implications for applications that require controlled degradation and predictable structural integrity over time, such as drug delivery, tissue engineering scaffolds, or temporary biomedical implants. The comparative analysis underscores the significance of polymer formulation in tailoring degradation kinetics and mechanical resilience (Fig. 2A).

3.2.2 Controlled and dose-dependent drug release over 35 days. The release profiles of 5-Fu from the electrospun PLGA membranes demonstrated a biphasic pattern: an initial burst phase followed by sustained drug release over 35 days (Fig. 2B).

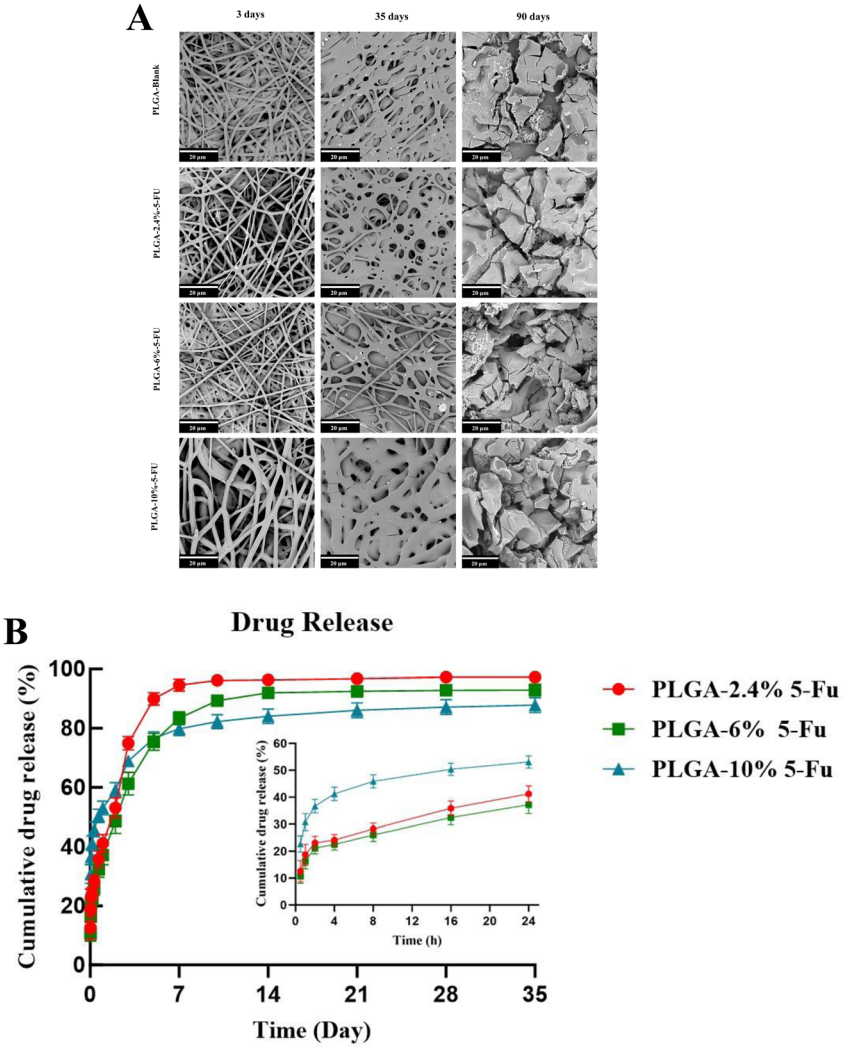

Fig. 2 Degradation-induced drug release. (A) SEM images illustrate the surface and structural evolution of multiple polymer scaffold formulations over the course of degradation, showing a progressive stage in the degradation timeline. Day 3 shows intact fibrous or porous architectures with well-defined structural features. As degradation progresses (35 days), the fibers appear thinner, pores expand, and the surface texture becomes smoother or more fragmented. The final stage (90 days) reveals substantial loss of structural integrity, including collapse of the network, plate-like fragmentation, or disintegration into smaller debris. Scale bars represent 20 μm for all images. (B) Drug release profiles of PLGA scaffolds with varying 5-Fu loadings over 35 days, with an inset depicting the early-phase release within 24 hours. Data are presented as mean ± SD ($n = 3$).

Open Access Article. Published on 02 January 2026. Downloaded on 4/7/2026 1:57:52 AM. This article is licensed under a Creative Commons Attribution-NonCommercial 3.0 Unported Licence.

The initial drug loading strongly influenced the extent and rate of release. The PLGA-2.4% 5-Fu membrane exhibited the highest burst release (~75% in the first 24 hours) and achieved nearly complete release (>95%) by day 7. In contrast, PLGA-10% 5-Fu membranes showed a more gradual release (~60% on day 1, ~85% by day 28), indicating enhanced release sustainability with higher drug content. The inset graph (Fig. 2B) illustrates early-phase kinetics, highlighting that increased drug loading mitigates the burst effect and prolongs drug availability. These results confirm the electrospun membranes' capacity to modulate drug release profiles, which are tunable and dose-responsive, positioning them as promising candidates for localized, sustained chemotherapeutic delivery systems.

Collectively, the electrospun PLGA scaffolds successfully encapsulated 5-Fu without compromising fiber morphology, and their tunable drug-release profiles underscore their potential as versatile platforms for controlled drug delivery. The correlation between drug loading, fiber morphology, and release kinetics provides a framework for optimizing scaffold design for specific clinical applications.

3.3 *In vitro* tumor inhibition

3.3.1 5-Fu-loaded PLGA electrospun scaffold inhibits tumor growth *in vitro*. The cytotoxic potential of 5-FU-loaded PLGA electrospun scaffolds was evaluated using the CCK-8 assay across multiple time points (24 h, 72 h, and 168 h) in both normal colonic epithelial cells (NCM460) and colorectal cancer cells (SW620). The experimental setup is schematically illustrated in Fig. 3A, where cells were cultured directly on PLGA fibrous membranes placed in 24-well plates, facilitating direct contact between the cells and the drug-loaded scaffold surface.

As shown in Fig. 3B, the NCM460 cells exhibited a reduction in cell viability upon exposure to PLGA scaffolds containing 5-FU. No concentration-dependent decline in cell viability was observed at all time points (24 h, 72 h, and 168 h). Notably, the PLGA-Blank group showed no statistically significant toxicity compared to the control, confirming that the scaffold material does not compromise cell viability.

In contrast, the SW620 colorectal cancer cells demonstrated a statistically significant reduction in viability with increasing 5-FU concentration in the PLGA scaffolds (Fig. 3B, lower panel). At 24 hours, a clear dose-dependent cytotoxic response was already evident, which was further amplified at 72 hours and 168 hours. Particularly at 168 hours, the PLGA-10%-5-FU group reduced cancer cell viability to less than 40%, underscoring the sustained release and potent antitumor activity of the drug-loaded fibers. This temporal decline in viability suggests that the effective prolonged delivery of 5-FU from the scaffold contributes to cumulative cytotoxic effects over time.

These findings highlight the differential sensitivity of normal and cancerous colon cells to 5-FU-loaded PLGA fibers, supporting their potential for localized chemotherapy with lesser toxicity to the surrounding environment. The dose- and time-dependent responses validate the scaffold's capability for controlled drug release, establishing it as a promising tool for colorectal cancer therapy.

To complement the quantitative cell viability analysis, qualitative assessment of cell morphology was conducted using live/dead fluorescence imaging of SW620 colorectal cancer cells cultured on PLGA scaffolds with varying concentrations of 5-FU over 24 h, 72 h, and 168 h (Fig. 3C). These images confirm the cytotoxic effects observed in the CCK-8 assay and provide additional insight into cellular behavior in response to localized drug delivery.

In the control and PLGA-Blank groups, cells exhibited progressive proliferation over time, as indicated by the increasing density and confluence of green fluorescence (representing live cells), particularly at 72 hours and 168 hours. By 168 h, cells in these groups formed continuous monolayers with widespread cytoplasmic spreading, indicative of robust adhesion, proliferation, and preserved morphology without cytotoxic stress. This observation also reinforces the biocompatibility of the PLGA scaffold material without chemotherapeutic loading.

In contrast, cells exposed to 5-FU-loaded scaffolds exhibited significantly reduced cell density and impaired spreading in a dose- and time-dependent manner. At 24 h, a notable decrease in viable cell count was observed in all 5-FU-loaded groups, particularly at the 6% and 10% concentrations. By 72 h, cells on PLGA-6%-5-FU and PLGA-10%-5-FU scaffolds appeared sparse, rounded, and showed limited adherence, consistent with early apoptotic morphology. At 168 h, the cytotoxic effect was most pronounced; cells on high-concentration scaffolds (especially 10% 5-FU) were nearly absent, with dark fields and disrupted fluorescence, suggesting substantial cell death and possible degradation of cellular remnants. The PLGA-2.4%-5-FU group, while exhibiting an intermediate response, still showed reduced proliferation and altered morphology compared to the control. The fluorescence imaging corroborates the CCK-8 assay results, affirming the potent and sustained antitumor efficacy of 5-FU-loaded electrospun PLGA scaffolds. The sharp contrast in morphological integrity between treated and untreated groups illustrates the effective release of the chemotherapeutic agent and the scaffold's capacity to confine cytotoxicity to malignant cells over extended durations. These findings support the use of PLGA-based drug delivery systems as a targeted therapeutic strategy for the treatment of localized colorectal cancer.

3.4 *In vivo* tumor inhibition

3.4.1 Tumor inhibition *via* 5-Fu-loaded PLGA electrospun scaffold. To evaluate the impact of different treatments on tumor progression, we measured tumor volume over 25 days following surgical intervention. The results revealed distinct patterns among the experimental groups (Fig. 4C). Wild-type control mice exhibited rapid tumor growth, reaching a peak volume of approximately 1500 mm^3 by day 25. In contrast, mice subjected to base membrane resection (BMR) showed a moderate reduction in tumor growth, with volumes plateauing at approximately 1000 mm^3. Intravenous (IV) administration of 5-FU further suppressed tumor growth, resulting in volumes of approximately 800 mm^3 by the endpoint.

Notably, localized delivery systems demonstrated superior efficacy. PLGA-blank implants (without drug) resulted in

 © 2026 The Author(s). Published by the Royal Society of Chemistry

Open Access Article. Published on 02 January 2026. Downloaded on 4/7/2026 1:57:52 AM.
This article is licensed under a Creative Commons Attribution-NonCommercial 3.0 Unported Licence.

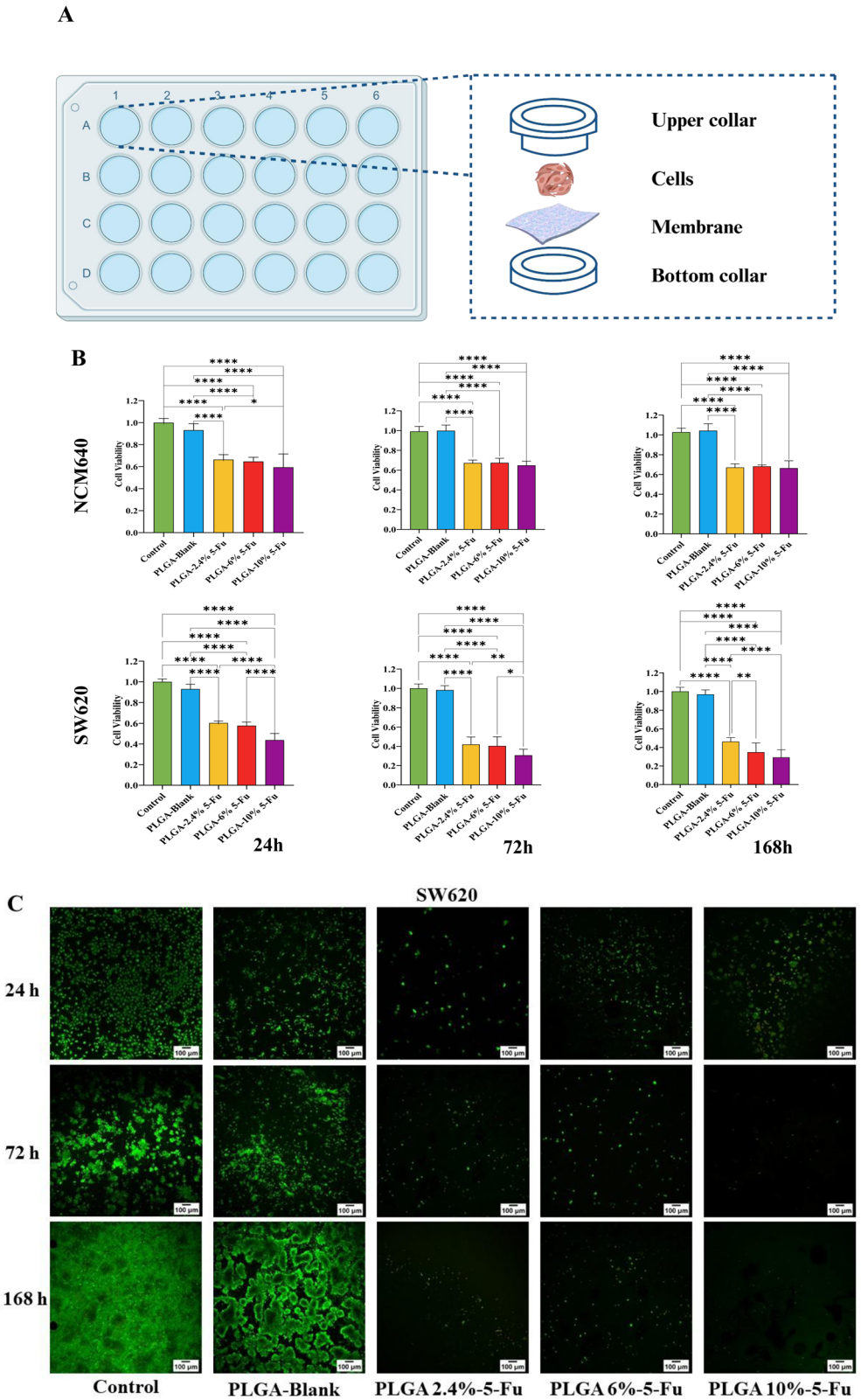

Fig. 3 *In vitro* cytotoxicity and live/dead cell analysis of 5-Fu-loaded PLGA electrospun scaffolds. (A) Schematic illustration of the transwell co-culture setup used to evaluate the effects of drug-loaded PLGA scaffolds on colorectal cancer (SW620) and normal colon epithelial (NCM460) cells. (B) Cell viability assay at 24, 72, and 168 h, showing a significant, dose-dependent reduction in cell survival with increasing 5-Fu content in the scaffolds (****$p < 0.0001$, ***$p < 0.001$, **$p < 0.01$). (C) Live/dead fluorescence staining of SW620 cells at different time points, demonstrating progressive cell death with higher drug loading and extended exposure times. Scale bar = 100 μm.

Open Access Article. Published on 02 January 2026. Downloaded on 4/7/2026 1:57:52 AM.
This article is licensed under a Creative Commons Attribution-NonCommercial 3.0 Unported Licence.

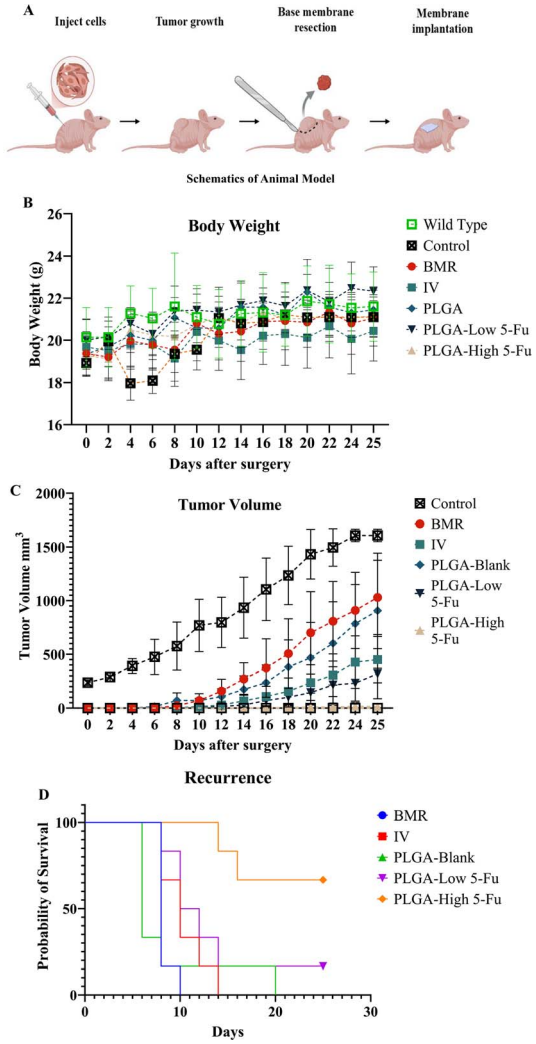

Fig. 4 *In vivo* therapeutic efficacy of 5-Fu-loaded PLGA electrospun scaffolds in a colorectal cancer mouse model. (A) Schematic illustration of the orthotopic colorectal tumor recurrence model, including cell implantation, tumor growth, base membrane resection, and scaffold implantation. (B) Body weight monitoring of mice across different treatment groups showed no significant systemic toxicity during the study period. (C) Tumor volume of untreated control, basemembrane resection (BMR), intravenous 5-FU (IV), PLGA-Blank scaffolds, PLGA-Low 5-FU scaffolds, and PLGA-High 5-FU scaffolds. Control tumors exhibited rapid expansion, reaching ~1700 mm^3 by day 25. BMR slowed early growth but still resulted in substantial tumor progression (~1000 mm^3 at day 25). IV 5-FU reduced tumor growth moderately, with final volumes of ~500–600 mm^3. PLGA-blank scaffolds produced a similar trajectory (~700–800 mm^3), indicating a minimal therapeutic effect in the absence of the drug. In contrast, PLGA-Low 5-FU significantly restricted tumor progression throughout the study, limiting mean tumor size to <300 mm^3 by day 25. The PLGA-High 5-FU group showed the most potent inhibition, with tumors remaining at near-baseline levels (≤50 mm^3) for the entire duration, exhibiting minimal measurable growth. Error bars represent mean ± SD, demonstrating consistent suppression of tumor proliferation with localized sustained 5-FU delivery from drug-loaded PLGA scaffolds. (D) Kaplan–Meier analysis of tumor recurrence probability, indicating significantly reduced recurrence in mice treated with drug-loaded scaffolds. The BMR and IV groups exhibited early recurrence, with median recurrence-free survival of ~7 and 9 days, respectively. PLGA-Blank showed slightly extended survival (~12 days). PLGA-Low 5-FU prolonged recurrence-free survival to ~18 days, while the PLGA-High 5-FU group maintained 60% recurrence-free survival through day 25, indicating substantial therapeutic advantage of localized, sustained-release 5-FU delivery.

a modest reduction compared to BMR, while PLGA-loaded formulations exhibited dose-dependent effects. PLGA-Low 5-FU reduced the tumor, and PLGA-High 5-FU achieved near-complete suppression after implantation. Overall, the two-way ANOVA analysis showed that tumor volumes in the BMR, IV, and PLGA-High 5-FU groups were significantly smaller than those in the control group ($p < 0.05$*). Furthermore, tumors in the PLGA-High 5-FU group were substantially smaller compared to all other experimental groups ($p < 0.05$), suggesting that the combination of high-dose 5-FU and PLGA delivery provides the most effective therapeutic outcome in this model.

The probability of recurrence was assessed over 24 days post-surgery (Fig. 4D). BMR alone was associated with a high recurrence rate (10% by day 10), underscoring the limitations of surgical resection as a standalone treatment. IV 5-FU delayed recurrence but reached 100% by day 14, while PLGA-blank implants showed delayed recurrence (100% recurrence by day 20). PLGA-5-Fu formulations significantly reduced recurrence, with PLGA-Low 5-Fu achieving 80% and PLGA-High 5-Fu achieving 30% at the endpoint.

3.4.2 Histological analysis after treatment. Histological analysis by Hematoxylin and Eosin (H&E) staining revealed distinct differences in tumor architecture and cellular morphology among the treatment groups. The control, BMR, and IV groups displayed dense tumor cell populations with prominent invasion into surrounding tissues, as indicated by the yellow arrows. In contrast, tumors treated with PLGA blank, PLGA-Low 5-Fu, and PLGA-High 5-Fu exhibited no cellular invasion (Fig. 5A). Immunohistochemical staining further demonstrated a significant decrease in Ki-67 expression, indicating suppressed proliferative activity in treated groups, particularly with high-dose PLGA-5-Fu scaffolds. Moreover, CD31 staining revealed diminished angiogenesis, while fibronectin staining showed reduced extracellular matrix remodeling and tumor invasion following treatment (Fig. 5B). These findings collectively confirm the therapeutic efficacy of localized 5-FU delivery *via* PLGA scaffolds in attenuating tumor growth and progression.

These results highlight the potential of PLGA-based drug delivery systems as a promising approach for enhancing chemotherapy efficacy. The significant inhibition of tumor growth observed with high-dose 5-FU delivered through PLGA is consistent with previous studies demonstrating the advantages of nanoparticle-based drug delivery in cancer therapy. The PLGA system enables the sustained and localized release of 5-FU, thereby enhancing drug exposure at the tumor site while minimizing systemic toxicity, ultimately leading to more effective treatment outcomes. While low-dose 5-FU also showed tumor growth inhibition, the effect was less pronounced, further supporting the idea that the combination of PLGA and high-dose 5-FU maximizes therapeutic efficacy. These findings suggest that PLGA-5-FU formulations could serve as an effective platform for improving the treatment of solid tumors. Future studies should focus on optimizing dosing regimens, investigating long-term survival benefits, and exploring the underlying mechanisms of action.

© 2026 The Author(s). Published by the Royal Society of Chemistry

Open Access Article. Published on 02 January 2026. Downloaded on 4/7/2026 1:57:52 AM.
This article is licensed under a Creative Commons Attribution-NonCommercial 3.0 Unported Licence.

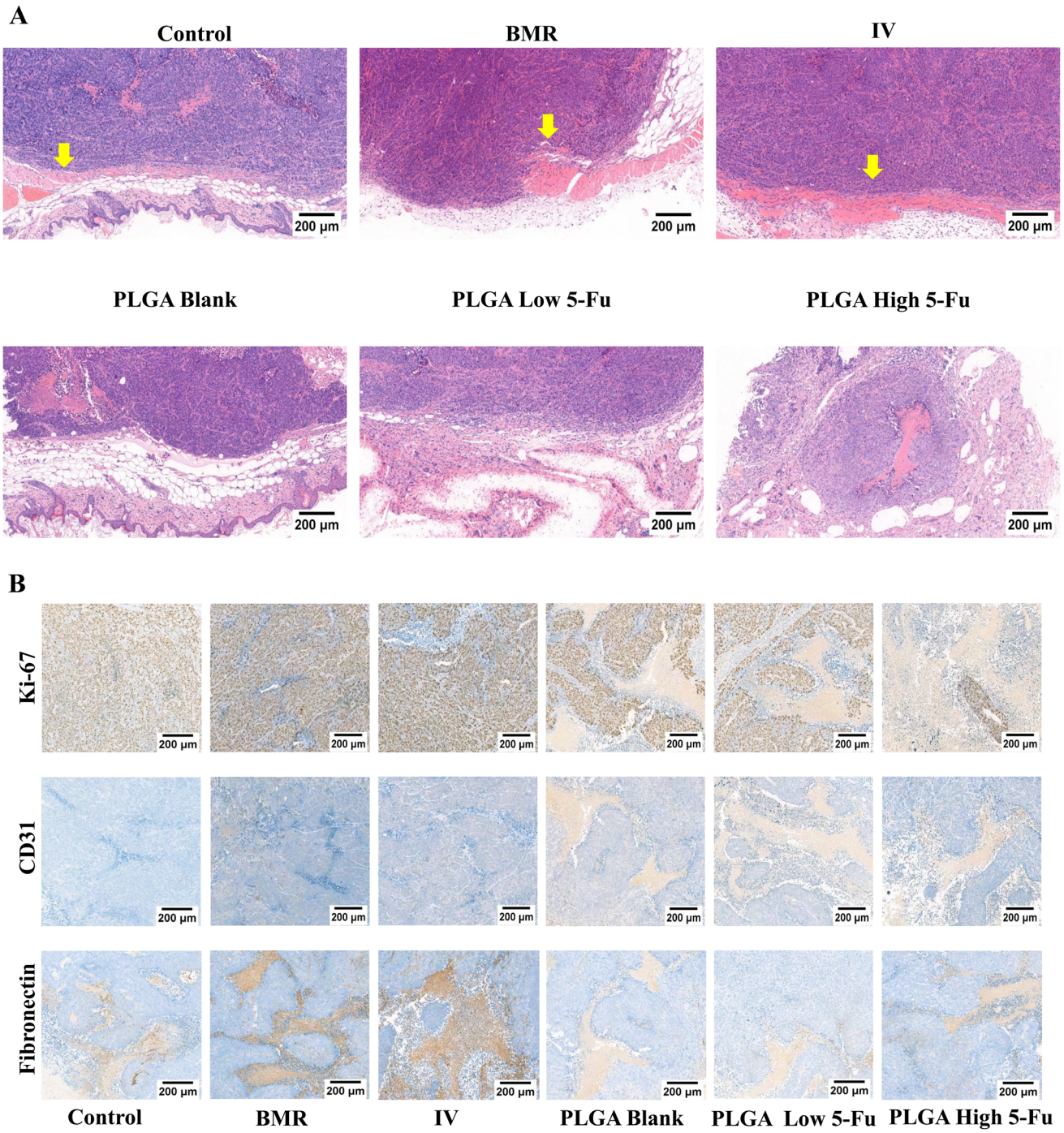

Fig. 5 Histopathological and immunohistochemical analyses of tumor tissues following treatment with 5-Fu-loaded PLGA electrospun scaffolds. (A) Hematoxylin and eosin (H&E) staining shows tumor architecture and cellular morphology across treatment groups, including control, BMR, IV 5-Fu, PLGA-Blank, PLGA-Low 5-Fu, and PLGA-High 5-Fu. Yellow arrows indicate the invasion of tumor cells into the surrounding tissue (B). Immunohistochemical staining for Ki-67 reveals markedly reduced proliferative activity in tumors treated with high-dose 5-FU-loaded scaffolds. CD31 staining demonstrates decreased angiogenesis and immune-associated activity, while fibronectin staining indicates suppressed extracellular matrix remodeling and tumor invasion in the treated groups. Scale bars are provided in the images.

4 Conclusion

This study presents a robust and tunable platform for localized chemotherapeutic delivery using electrospun PLGA fibrous scaffolds loaded with 5-fluorouracil (5-FU), offering a promising alternative to systemic chemotherapy for colorectal cancer. By leveraging the structural versatility of electrospinning, we successfully engineered drug-eluting scaffolds capable of sustained and spatially confined drug release, while preserving biocompatibility and mechanical integrity. The scaffolds exhibited a well-defined, dose-dependent cytotoxic effect against colorectal cancer cells, with minimal impact on normal

Open Access Article. Published on 02 January 2026. Downloaded on 4/7/2026 1:57:52 AM. This article is licensed under a Creative Commons Attribution-NonCommercial 3.0 Unported Licence.

colonic epithelial cells, demonstrating therapeutic selectivity and potential clinical safety.

The ability to modulate fiber morphology and drug release kinetics through simple adjustments in drug loading provides a powerful design principle for tailoring therapeutic outcomes. Furthermore, live/dead imaging confirmed long-term suppression of tumor cell viability, reinforcing the translational relevance of this localized drug delivery strategy for postoperative tumor inhibition or as an implantable adjuvant therapy.

However, this study is limited to *in vitro* assessment and *in vivo* subcutaneous model.*In vivo* evaluation in orthotopic or post-resection models is necessary to validate pharmacokinetics, biodistribution, immune interactions, and therapeutic efficacy within complex biological environments. Additionally, long-term degradation kinetics and scaffold–host interactions remain to be fully elucidated. This study establishes a foundational framework for developing intelligent, site-specific chemotherapeutic scaffolds, with broad implications for personalized oncology and regenerative medicine.

This study presents a biodegradable, implantable PLGA nanofiber scaffold engineered for localized, sustained delivery of 5-FU to suppress colorectal cancer progression and postoperative recurrence. By optimizing drug loading within electrospun PLGA fibers, we achieved a tunable morphology and controlled long-term release profiles that maintain therapeutic drug concentrations over several weeks. This sustained exposure translated into potent, dose-dependent inhibition of colorectal cancer cells *in vitro*, with minimal cytotoxicity toward normal colonic epithelial cells, demonstrating the therapeutic selectivity of the scaffold system.

In a clinically relevant tumor-recurrence mouse model, the 5-FU-loaded scaffolds significantly reduced tumor regrowth and lowered recurrence rates compared with systemic chemotherapy or surgery alone. Histological and immunohistochemical analyses confirmed reductions in tumor proliferation, angiogenesis, and extracellular matrix remodeling, indicating robust suppression of tumor-promoting microenvironmental features. Importantly, the scaffolds were well tolerated, with no observable systemic toxicity.

When compared with currently available localized drug-delivery platforms such as hydrogels, microspheres, and external infusion systems, our scaffold exhibits several distinctive advantages. First, its design enables seamless intraoperative placement without reliance on auxiliary hardware or specialized delivery instruments. The PLGA-based architecture confers reproducible, extended release kinetics, allowing for controlled therapeutic exposure over clinically meaningful timeframes. In addition, the scaffold's mechanical robustness and capacity for conforming to irregular resection margins support precise positioning within the postoperative cavity. The system also accommodates tunable drug-loading, permitting adaptation to different therapeutic requirements and pathological contexts. Its fully biodegradable composition ensures complete resorption without residual material, thereby obviating the need for secondary removal procedures. Our study presents a novel approach distinct from previous research in several key aspects. Notably, our drug release profile demonstrates a sustained release over a period of up to 35 days, which is significantly longer than the shorter release durations commonly reported in existing literature.[18] In addition, while most studies focus on cell viability assays conducted over a 24- to 48-hour period, no animal studies[33,34], our assays extend over 7 days, providing a more comprehensive assessment of the long-term effects of the material.

Furthermore, our animal model study spans 5 weeks, which contrasts with typical experimental designs that focus either on *in vitro* studies only[34–38] or primarily on the implantation of materials in tumor models for relatively shorter durations. Unlike existing studies that mainly address tumor treatment, our material is specifically designed to offer extracellular matrix (ECM) support and prevent recurrence following surgical intervention. This functional emphasis on postoperative recurrence inhibition further distinguishes our approach from conventional cancer therapies. These differences underscore the novelty and uniqueness of our study, which aims to provide a sustained therapeutic effect and long-term benefits beyond the tumor site itself.

Together, these findings underscore the translational promise of 5-FU-eluting PLGA scaffolds as a practical and effective strategy for managing postoperative colorectal cancer. Future studies will focus on evaluating long-term *in vivo* degradation behavior, immune responses, combination-drug loading, and potential extension of this platform to other solid tumors. This work lays the foundation for the development of next-generation, site-specific chemotherapeutic implants designed to enhance local tumor control and reduce recurrence after surgery.

Conflicts of interest

The authors declare no competing interests.

Data availability

All relevant data and findings of this study are provided in the article. Additional raw datasets are available from the corresponding author upon reasonable request.

Acknowledgements

This work was financially supported by Shenzhen Medical Research Fund (D2402004), Ningbo Bureau of Science and Technology (2024Z033), Ningbo Bureau of Science and Technology (2023Z187), Shenzhen Science and Technology Innovation Project (JCYJ20210324095802006), Shenzhen University (2023YG027), Medical Science and Technology Foundation of Guangdong Province (2023102514345235), Guangdong Medical Scientific Research Found (A2024591), Dongguan Science and Technology of Social Development Program (20231800937512), Guangdong Basic and Applied Basic Research Foundation (2024A1515140042), Talent Development Foundation of The First Dongguan Affiliated Hospital of Guangdong Medical University (PU2024005). This work was also financially

 © 2026 The Author(s). Published by the Royal Society of Chemistry

Open Access Article. Published on 02 January 2026. Downloaded on 4/7/2026 1:57:52 AM. This article is licensed under a Creative Commons Attribution-NonCommercial 3.0 Unported Licence.

supported by Kingfa SCI. & TECH. CO., LTD (2023149), Ningbo Guangyuan Zhi Xin Biotechnology. Co., Ltd (2023202).

References

1 F. Bray, M. Laversanne, H. Sung, J. Ferlay, R. L. Siegel, I. Soerjomataram and A. Jemal, *CA Cancer J Clin.*, 2024, **74**, 229–263.
2 Y. Zheng, R. Zhou, J. Cai, N. Yang, Z. Wen, Z. Zhang, H. Sun, G. Huang, Y. Guan, N. Huang, M. Shi, Y. Liao, J. Bin and W. Liao, *Cancer Res.*, 2023, **83**, 3577–3592.
3 E. Chen and W. Zhou, *Crit. Rev. Oncol./Hematol.*, 2025, **212**, 104775.
4 W. H. Gmeiner and C. C. Okechukwu, *Cancer Drug Resist.*, 2023, **6**, 257–272.
5 A. B. Benson, A. P. Venook, M. Adam, G. Chang, Y. J. Chen, K. K. Ciombor, S. A. Cohen, H. S. Cooper, D. Deming, I. Garrido-Laguna, J. L. Grem, P. Haste, J. R. Hecht, S. Hoffe, S. Hunt, H. Hussan, K. L. Johung, N. Joseph, N. Kirilcuk, S. Krishnamurthi, M. Malla, J. K. Maratt, W. A. Messersmith, J. Meyerhardt, E. D. Miller, M. F. Mulcahy, S. Nurkin, M. J. Overman, A. Parikh, H. Patel, K. Pedersen, L. Saltz, C. Schneider, D. Shibata, B. Shogan, J. M. Skibber, C. T. Sofocleous, A. Tavakkoli, C. G. Willett, C. Wu, L. A. Gurski, J. Snedeker and F. Jones, *J. Natl. Compr. Cancer Network*, 2024, **22**(2D), e240029.
6 M. Lashof-Sullivan, A. L. McSweeney, D. T. Ting, M. P. Kim, C.-W. D. Tzeng and L. Indolfi, *Cancer Res.*, 2019, **79**, B26.
7 J. Mielko, K. Rawicz-Pruszyński, M. Skórzewska, B. Ciseł, A. Pikuła, M. Kwietniewska, K. Gęca, K. Sędłak, A. Kurylcio and W. P. Polkowski, *Cancers*, 2019, **11**(11), 1715.
8 A. M. Sonabend, R. M. Stuart, J. Yun, T. Yanagihara, H. Mohajed, S. Dashnaw, S. S. Bruce, T. Brown, A. Romanov, M. Sebastian, F. Arias-Mendoza, E. Bagiella, P. Canoll and J. N. Bruce, *Neuro-Oncology*, 2011, **13**, 886–893.
9 Y. J. Lin, C. C. Chen, D. Nguyen, H. R. Su, K. J. Lin, H. L. Chen, Y. J. Hu, P. L. Lai and H. W. Sung, *Small*, 2020, **16**, e2000655.
10 S. Karaosmanoglu, M. Zhou, B. Shi, X. Zhang, G. R. Williams and X. Chen, *J. Control. Release*, 2021, **329**, 805–832.
11 D. Wu, Z. Q. Zhu, H. X. Tang, Z. E. Shi, J. Kang, Q. Liu and J. Qi, *Theranostics*, 2020, **10**, 9808–9829.
12 M. Wiranowska, R. Toomey, R. Falahat and N. Alcantar, *Cancer Res.*, 2019, **79**, 3615.
13 J. Hu, J. Wei, W. Liu and Y. J. J. O. B. S. Chen, *Polym. Edn.*, 2013, **24**, 972–985.
14 D. Han, M. Sasaki, H. Yoshino, S. Kofuji, A. T. Sasaki and A. J. Steckl, *J. Drug Delivery Sci. Technol.*, 2017, **40**, 45–50.
15 Y. Zhang, J. Yu, H. N. Bomba, Y. Zhu and Z. Gu, *Chem. Rev.*, 2016, **116**, 12536–12563.
16 M. Saif Ur Rahman, J. Wu, H. Chen, C. Sun, Y. Liu and S. Xu, *Adv. Phys.:X*, 2023, **8**, 2153624.
17 C. Shih-Feng, C. Daniel and A. W. Kim, *J. Controlled Release*, 2015, **220**, 584–591.
18 S. Abid, T. Hussain, Z. A. Raza and A. Nazir, *Mater Sci Eng C Mater Biol Appl.*, 2019, **97**, 966–977.
19 A. Haider, S. Haider and I.-K. Kang, *Arabian J. Chem.*, 2018, **11**, 1165–1188.
20 K. Kim, M. Yu, X. Zong, J. Chiu, D. Fang, Y.-S. Seo, B. S. Hsiao, B. Chu and M. Hadjiargyrou, *Biomaterials*, 2003, **24**, 4977–4985.
21 N. Monteiro, M. Martins, A. Martins, N. A. Fonseca, J. N. Moreira, R. L. Reis and N. M. Neves, *Acta Biomater.*, 2015, **18**, 196–205.
22 S. Amini, H. Ebrahimzadeh, S. Seidi and N. Jalilian, *Food Chem.*, 2021, **350**, 129242.
23 D. Tian, X. Lu, Y. Zhu, M. Li and C. Wang, *J. Power Sources*, 2019, **413**, 50–58.
24 U. Mahmood, A. S. Alkorbi, T. Hussain, A. Nazir, M. B. Qadir, Z. Khaliq, S. Faheem and M. Jalalah, *RSC Adv.*, 2024, **14**, 5959–5974.
25 J. Wu, S. Xu, C. C. Han and G. Yuan, *J. Control. Release*, 2021, **331**, 472–479.
26 S. Huang, Y. Zhang, C. Wang, Q. Xia, M. Saif Ur Rahman, H. Chen, C. Han, Y. Liu and S. Xu, *Int. J. Mol. Sci.*, 2022, **23**(4), 2185.
27 M. S. Ur Rahman, L. Zhang, L. Wu, Y. Xie, C. Li and J. Cao, *Drug Des., Dev. Ther.*, 2017, **11**, 2431–2441.
28 H. Chen, J. Wu, M. S. U. Rahman, S. Li, J. Wang, S. Li, Y. Wu, Y. Liu and S. Xu, *Biomater. Adv.*, 2023, **148**, 213358.
29 R. Zhang, X. Q. Song, R. P. Liu, Z. Y. Ma and J. Y. Xu, *J. Med. Chem.*, 2019, **62**, 4543–4554.
30 L. Fang, Y. Jiang, Y. Yang, Y. Zheng, J. Zheng, H. Jiang, S. Zhang, L. Lin, J. Zheng, S. Zhang and X. Zhuang, *Oncotarget*, 2016, **7**, 81880–81887.
31 M. J. O'connell, J. A. Martenson, H. S. Wieand, J. E. Krook, J. S. Macdonald, D. G. Haller, R. J. Mayer, L. L. Gunderson and T. A. Rich, *N. Engl. J. Med.*, 1994, **331**, 502–507.
32 T. André, A. De Gramont, D. Vernerey, B. Chibaudel, F. Bonnetain, A. Tijeras-Raballand, A. Scriva, T. Hickish, J. Tabernero and J. L. Van Laethem, *J. Clin. Oncol.*, 2015, **33**, 4176–4187.
33 D. Xie, P. Ma, X. Ding, X. Yang, L. Duan, B. Xiao and S. J. Yi, *Front. Bioeng. Biotechnol*, 2021, **8**, 618516.
34 Y. Zhao, X. Ma, H. Xu, H. Long, M. Zou, W. Qi and J. Zhou, *Int. J. Polym. Mater. Polym. Biomater*, 2025, 1–10.
35 L. Zavagna, E. F. Canelli, B. Azimi, F. Troisi, L. Scarpelli, T. Macchi, G. Gallone, M. Labardi, R. Giovannoni and M. Milazzo, *Macromol. Mater. Eng.*, 2024, **309**, 2400123.
36 J. Dai, J. Jin, S. Yang and G. Li, *Mater. Res. Express*, 2017, **4**, 075403.
37 C. Ricci, B. Azimi, L. Panariello, B. Antognoli, B. Cecchini, R. Rovelli, M. Rustembek, P. Cinelli, M. Milazzo, S. Danti and A. Lazzeri, *Int. J. Mol. Sci.*, 2023, **24**(11), 9443.
38 J. Zhang, X. Wang, T. Liu, S. Liu and X. Jing, *Drug Delivery*, 2016, **23**, 794–800.

© 2026 The Author(s). Published by the Royal Society of Chemistry